ACS APPLIED MATERIALS & INTERFACES

Letter

www.acsami.org

Plasmonic Metal-to-Semiconductor Switching in Au Nanorod-ZnO nanocomposite films

Fei Wu,[†] Limei Tian,[†] Ravindra Kanjolia,[‡] Srikanth Singamaneni,[†] and Parag Banerjee*[,†]

[†]Department of Mechanical Engineering and Materials Science, Washington University in St. Louis, One Brookings Drive, St. Louis, Missouri 63130, United States

[‡]SAFC Hitech, 1429 Hilldale Avenue, Haverhill, Massachusetts 01832, United States

Supporting Information

ABSTRACT: We demonstrate conductivity switching from a metal to semiconductor using plasmonic excitation and charge injection in Au-nanorod (AuNRs)-ZnO nanocomposite films. ZnO films 12.6, 20.3, and 35.6 nm were deposited over AuNRs using atomic layer deposition. In dark conditions, the films transitioned from metallic to semiconducting behavior between 150 and 200 K. However, under sub-bandgap, white light illumination, all films behaved as semiconductors from 80 to 320 K. Photoresponse (light/dark conductivity) was strongly dependent on the thickness of ZnO, which was 94.4 for AuNR−12.6 nm ZnO and negligible for AuNR−35.6 nm ZnO. Conductivity switching and thickness dependence of photoresponse were attributed to plasmonically excited electrons injected from AuNRs into ZnO. Activation energies for conduction were extracted for these processes.

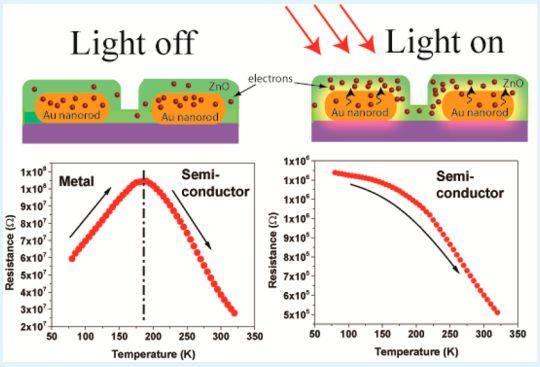

KEYWORDS: *plasmon enhancement, atomic layer deposition, Au nanorods, temperature dependent conductivity, photoresponse, ZnO*

1. INTRODUCTION

Photon management using plasmonics is a new method to trap and absorb light inside various semiconductor thin films and nanostructures.[1−4] Shape-controlled Au nanostructures have been extensively studied, because of their localized surface plasmon resonance (LSPR) in the visible and near infrared parts of the electromagnetic (EM) spectrum.[1,5−7] Recently,[8,9] it has been shown using a layered combination of Au nanoparticles (NPs) and TiO_2 film, that light absorption and resultant photoresponse can be made to map the spectral behavior of the plasmon resonance in the AuNPs rather than the fundamental absorption mode (3.3 eV) of the TiO_2 thin film. Thus, this approach decouples a film's ability to absorb light (governed by its bandgap, $E_g \sim 3.3$ eV) from its optoelectronic response. Further, increased light absorbance while lowering film thicknesses has provided a promising way to improve photocurrent responses and overall efficiencies of energy harvesting devices such as photocatalytic, photoelectrochemical, and dye-sensitized solar cells.[4,8,10−12]

In this letter, we report on the temperature-dependent (80 K-320 K) conductivity behavior of Au nanorod (AuNR)-ZnO nanocomposite films under dark and sub-bandgap (<3.3 eV), white light illumination conditions. Temperature-controlled conductivity provides information on the energetics of the charge transport processes (specifically activation energy, E_a) and can help elucidate plasmon-induced mechanisms of charge conduction. Such analysis assumes special relevance, especially under sub-bandgap illumination conditions when only defect mediated conductivity mechanisms are active and plasmonic interactions with thermally activated conductivity pathways can therefore be controllably studied.

AuNRs are particularly attractive considering the facile and large tunability of the LSPR wavelength of nanorods with high aspect ratio and sharp corners, which form electromagnetic hot-spots.[13−16] As a "blanket film", we choose ZnO because of its high optical transmittance and wide bandgap (3.3 eV). Further, atomic layer deposition (ALD) is used as a technique to deposit ZnO since ALD provides strict, monolayer thickness control of the film, crucial for studying the impact of near-field effects produced as a result of plasmonic interaction of metal NPs with semiconductor films.

2. EXPERIMENTAL SECTION

AuNRs were synthesized using a seed-mediated approach.[17,18] The AuNRs were stabilized using cetyltrimethylammonium bromide (CTAB). Glass substrates modified with (3-mercaptopropyl) triethoxysilane (MPTES) were subsequently exposed to the AuNR solution followed by rinsing with water to remove loosely bound NPs (details in the Supporting Information, Section S1). The exposure times for AuNR attachment were 2 h for low density and 48 h for high density AuNRs adsorbed on substrate.[13] ALD of ZnO was carried on substrates attached with low and high density AuNR substrates in a customized, home-built reactor. Diethyl Zn (DEZ) and

Received: June 14, 2013
Accepted: August 2, 2013
Published: August 2, 2013

   dx.doi.org/10.1021/am402309x | ACS Appl. Mater. Interfaces 2013, 5, 7693−7697

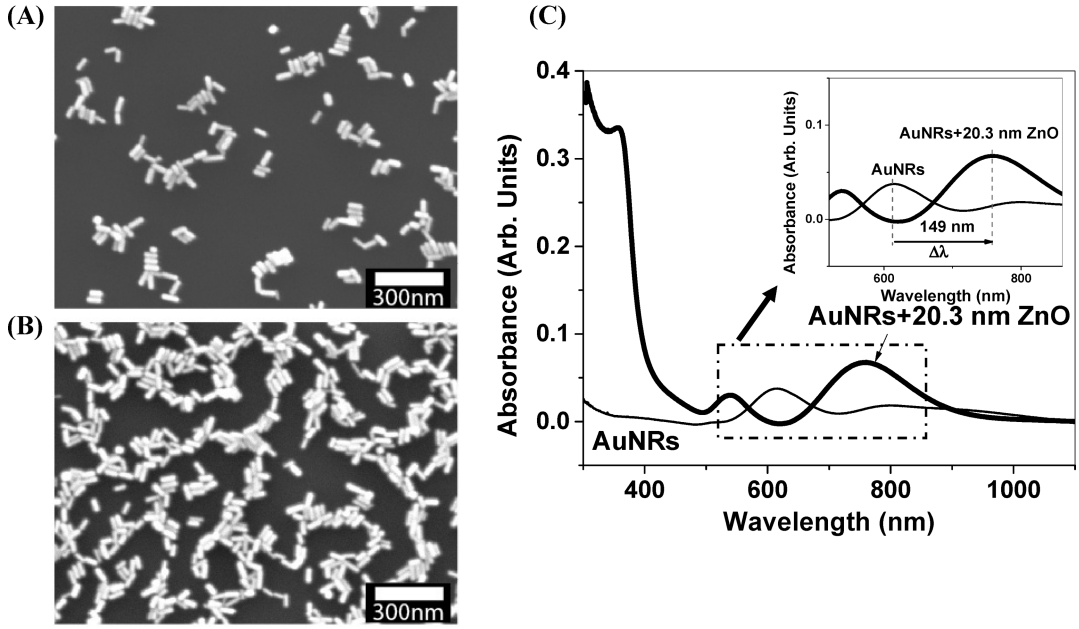

Figure 1. SEM images of (A) low density and (B) high density AuNRs. The AuNRs are 70 nm in length and 24 nm in diameter. The area coverage for the low and high density is 10.2% and 36.4%, respectively. (C) UV−vis data for low density AuNR with and without 20.3 nm ZnO shows the high absorbance due to ZnO for λ < 400 nm in the AuNR-20.3 nm ZnO sample and a corresponding red shift in the coupled LSPR peak from 614 nm for the AuNR sample to 763 nm. Plasmonic resonance peak shift was enlarged and put on the right corner.

H_2O were used as precursors and the temperature of deposition was 150 °C. A deposition rate of 1.7 Å/Cy was obtained in line with reported values.[19] The thickness of the ZnO were 12.6 nm, 20.3 nm 35.6 nm, measured using ellipsometry (α-SE, Woollam). Au/Cr electrodes were patterned using a shadow mask with "□" patterns 1 mm × 1 mm separated by 780 μm channel length in a thermal evaporator. A JANIS probe station (ST500-1-2CX) was used to measure the channel resistance in the samples from 80 K to 320 K with a step of 5 K. A Keithley 2400 Source Measure Unit was used to measure resistance. The average pressure of the chamber was maintained at or below 1×10^{-2} mTorr. Light measurements were performed by cooling the sample to 80K, then turning the light source ON for the temperature ramp from 80K to 320K. An Edmund optics (MI150) lamp provided white light with a power intensity of 5.7 mW/cm^2 (see the Supporting Information, Figure S2). The lamp provided negligible energy for λ < 400 nm. A JEOL 7001LVF SEM was used to characterize the AuNRs. UV−vis spectra of the samples were obtained on a Shimadzu UV-1800.

3. RESULTS

The size and distribution of low- and high-density AuNRs with a length of ∼70 nm and diameter of ∼24 nm are shown in images A and B in Figure 1. An average density of 0.52×10^{10} /cm^2 (area coverage 10.2%) for low-density AuNRs and 1.41×10^{10} /cm^2 (area coverage 36.4%) for high-density AuNRs were calculated. It was confirmed using AFM that upon ALD, conformal ZnO deposition on AuNRs occurred (see the Supporting Information, Figure S3).

UV−vis spectra of the low-density AuNR before and after 20.3 nm ZnO deposition is shown in Figure 1C. Two effects can clearly be seen upon ZnO deposition. First, the coupled plasmon peak at 614 nm red-shifts to 763 nm indicating the effect of increased dielectric constant (air → ZnO) surrounding AuNRs. Second, the ZnO absorption band (increased absorbance for λ < 400 nm) is observed. Both these effects show that the AuNRs and the ZnO film actively contribute to the optical response of the nanocomposite film.

Conductivity vs. 1/temperature (σ vs. $1/k_BT$, k_B = Boltzmann constant) measurements are shown in Figure 2A under dark (filled symbols) and light (open symbols) conditions. Photoresponse (ratio of light over dark σ) due to sub-bandgap, white light illumination increases as thickness of ZnO film increases. The maximum photoresponse observed was 1.15, 1.25, and 1.47 for the 12.6, 20.3, and 35.6 nm thick ZnO films, respectively. Thicker films having higher optical path lengths for photons should have higher absorption and hence higher excitation from traps upon illumination.[20]

σ vs. $1/k_BT$ for low-density AuNRs coated with 12.6, 20.3, and 35.6 nm ZnO is shown in Figure 2B. Surprisingly, an enhancement of 94.4 was seen for low-density AuNRs-12.6 nm ZnO sample, whereas low-density AuNRs-20.3 nm ZnO obtained 1.36 light enhancement. Dark and light conductance differed only slightly for low-density AuNR-35.6 nm ZnO films.

In Figure 2C, the photoresponse of 20.3 nm ZnO, low-density AuNR−20.3 nm ZnO, and high-density AuNR−20.3 nm ZnO films demonstrates that increased AuNR densities can only modestly increase the light response of the nanocomposite films. The maximum photoresponse were 1.25 to 1.36 and to 1.40 for ZnO, low-density, and high-density AuNR−ZnO films, respectively. However, the effect of AuNR density on 12.6 nm ZnO did not yield a similar trend. The maximum photoresponse (not shown) for 12.6 nm ZnO, low-density AuNR−12.6 nm ZnO, and high-density AuNR−12.6 nm ZnO was 1.15, 94.4, and 55.5, respectively.

4. DISCUSSION

Because of the large variation in ρ across samples (from 1×10^8 to 1×10^3 Ω) , we plot "normalized" ρ vs. T for ease of comparison. The normalized resistance is plotted from 0 to 1 by assigning the lowest resistance a "0" and the highest

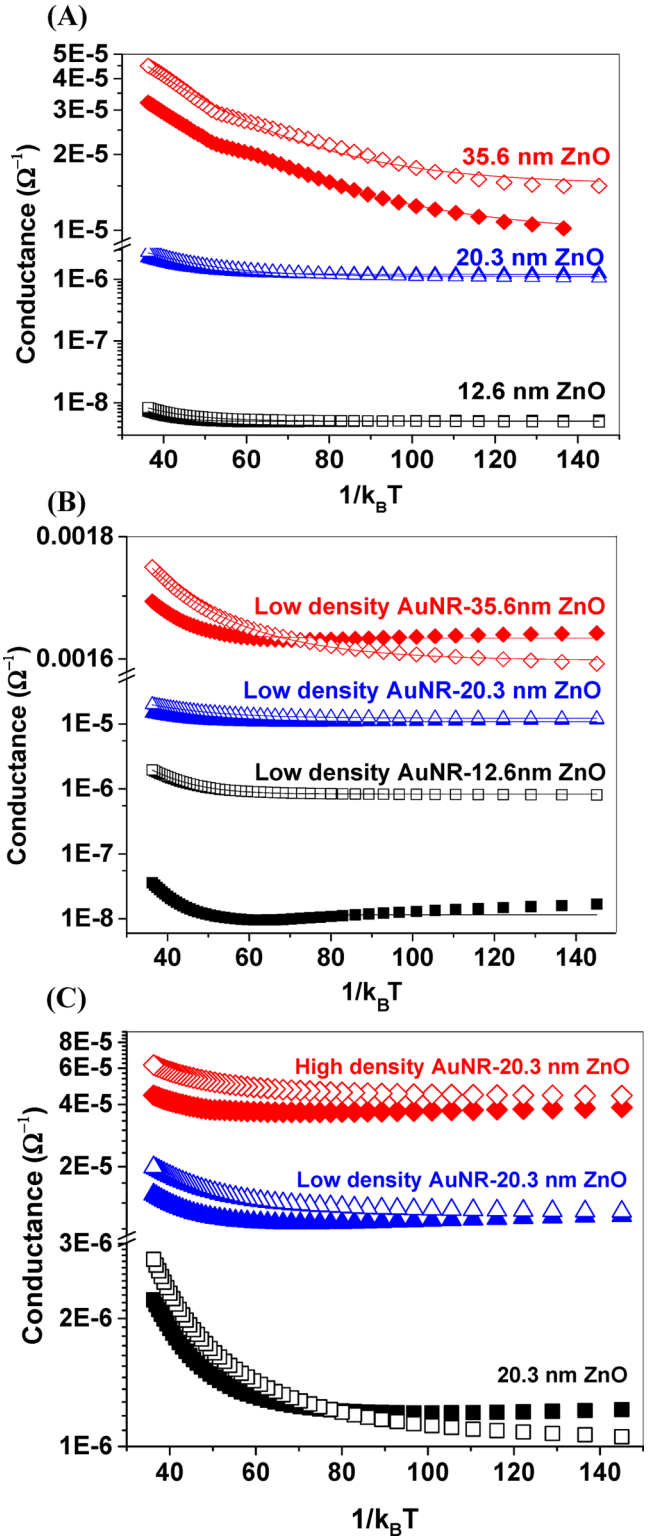

Figure 2. Conductance vs. $1/k_BT$ curves under dark (solid symbol) and white light (open symbol) for (A) 12.6 nm (□), 20 nm (Δ), and 35.6 nm (◇) ZnO; (B) low-density AuNRs with 12.6 nm (□), 20 nm (Δ), and 35.6 nm (◇) ZnO on top; and (C) 20.3 nm ZnO (□), low-density AuNR + 20.3 nm ZnO (Δ), and high-density AuNR + 20.3 nm ZnO (◇).

resistance a "1". Such an analysis clearly delineates regions of metallic and semiconductor behavior.

In Figure 3A, normalized ρ vs. T is plotted for low-density AuNR with 12.6, 20.3, and 35.6 nm ZnO films. In all three samples, dark measurements (filled symbols) showed an initial metallic behavior (ρ rises as T increases). At higher temperatures, ρ switches to a thermally activated mechanism (ρ decreases with increase in T). This mixed ρ behavior shows that AuNRs determine conductivity in the absence of thermal excitation of defects in the ZnO film. However, under white light illumination, all films switch to semiconducting behavior for the entire temperature range.

A plot of normalized ρ vs. T for various AuNR densities + ZnO nanocomposite films in Figure 3B indicates that although a pure ZnO film has monotonically decreasing ρ as T increases for both dark and light conditions, incorporating AuNR into the ZnO creates the characteristic metal to semiconductor transition for dark conditions. Both high and low-density AuNR + ZnO films have overlapping dark resistivity indicating little effect of AuNR density on the normalized ρ vs. T behavior. Upon illumination, the composite films behave as semiconductors across the entire temperature range.

The mixed mode resistance in dark can be modeled using an equivalent parallel circuit consisting of a "metallic" component and ZnO. The resistance, ρ in dark of the circuit is given as

$$\rho_{\text{dark}} = \left[\frac{1}{\rho_{\text{metallic}}[1 + \alpha(T - 298)]} + \frac{1}{A\exp\left(\frac{E_a}{k_BT}\right)} \right]^{-1}$$

Here, ρ_{metallic} is the resistance of the metallic component at 298 K, α is the temperature coefficient of resistivity, A is the pre-exponential term and Ea the activation energy for conductivity in ZnO. For resistance modeling in light, a single E_a based Arrhenius relationship is used to model the temperature dependence, i.e., $\rho_{\text{light}} = A\ \exp(E_a/k_BT)$. We differentiate between a metallic conduction pathway and a AuNR pathway because in our set of experiments the AuNR do not form percolation pathways between the two testing electrodes. Thus, the AuNR must couple with the intermediate ZnO film to form metallic channel.

On the basis of the equations above, three regimes of conduction can be isolated. For dark and 80 K < $T \lesssim$ 200 K, metallic pathway is the preferred path of conduction (Figure 4A). For dark and ~200 K < T < 320 K, ZnO conduction is higher than the AuNR and therefore dominates the nanocomposite response (Figure 4B). Finally, under illumination, ZnO conductivity dominates nanocomposite response for 80 K < T < 320 K (Figure 4C).

The maximum photoresponse and extracted parameters ρ_{metallic}, α, and E_a are provided in Table 1 for ZnO only and AuNR-ZnO films. An adjusted r^2 of >0.99 is obtained in all cases. It is to be noted that α varies from 3×10^{-3} K^{-1} for the low density AuNR-12.6 nm ZnO to 1.3×10^{-4} K^{-1} for the low-density AuNR−35.6 nm ZnO film, whereas α for bulk Au is 3.4×10^{-3} K^{-1}. This further leads credence to the fact that the metallic pathway consists of a combination of AuNR and intermediate ZnO. It is possible that because of the large shape anisotropy (aspect ratio of 3:1) of the AuNRs, application of a voltage creates high electric fields at their terminal ends (long axis) of the AuNRs. Electrons get injected and tunnel across the intermediate ZnO because of these high fields and thus create metallic behavior in these films.

dx.doi.org/10.1021/am402309x | ACS Appl. Mater. Interfaces 2013, 5, 7693−7697

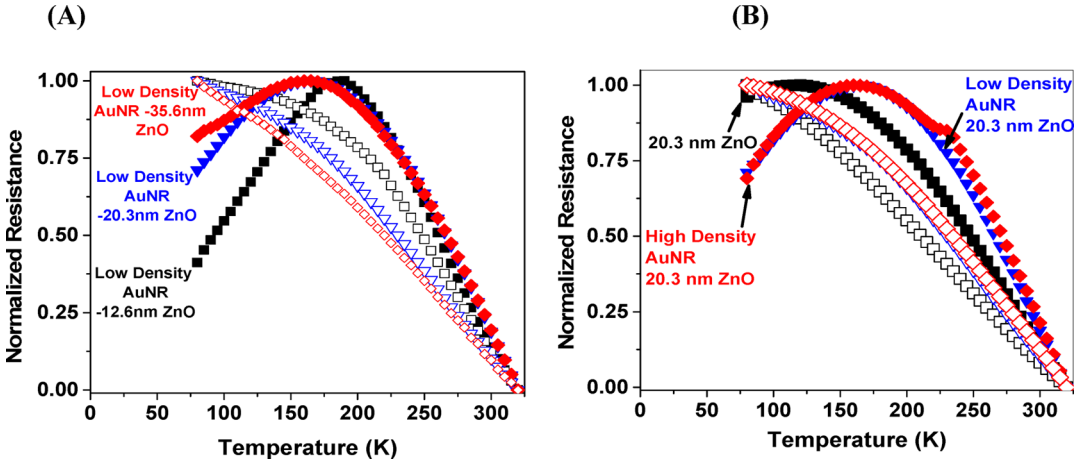

Figure 3. Normalized resistance vs. temperature in dark (solid) and white light (open) conditions for (A) low-density AuNR with different ZnO thickness and (B) pure ZnO and ZnO with low- and high-density AuNRs. In cases where the AuNR is embedded in the ZnO, dark conductivity always shows a metal to semiconductor transition (150−200 K). However, upon illumination, all samples become semiconducting.

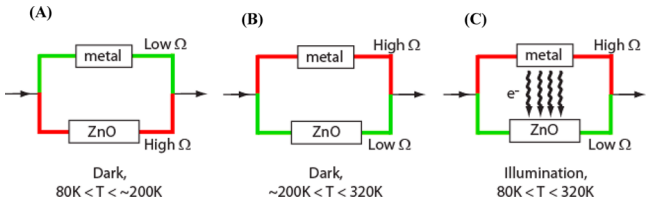

Figure 4. (A) Proposed equivalent circuit for AuNR−ZnO nanocomposite thin films consists of two parallel resistive elements of a metal and ZnO. In dark and for 80 K < $T \lesssim$ 200 K, the metallic pathway remains a more conducting (green) path B) For ~200 K < T < 320 K, the ZnO conductivity increases (green) due to the thermal excitation of charge carriers in the ZnO and the ZnO dominates the conductivity behavior of the film (C) Under white light sub-bandgap illumination, plasmons produced on the AuNR surface inject electrons into the ZnO making it highly conducting (green) across the entire temperature range (80 K < T < 320 K).

Dark E_a decreases with an increase in film thickness for ZnO films (183 to 33 meV) and for AuNR + ZnO films (137 to 72 meV). This thickness dependency of E_a is due to surface-adsorbed species such as O_2^- on ZnO which produces a depletion region (W_d) inside ZnO.[21,22] W_d is calculated to be 17.6 nm (see the Supporting Information, Section S4). Thus, 12.6 nm ZnO films are fully depleted. For AuNR + ZnO films the AuNR/ZnO interface can produce a Schottky barrier further depleting the film.[23] Upon illumination, E_a drops indicating a flattening of the ZnO band structure in the vicinity of the surface (for ZnO only and AuNR + ZnO films) and AuNR/ZnO (for AuNR + ZnO films) interface because of (1) high electric fields as a result of plasmonic near field effects and (2) excess carrier generation and injection.

On the basis of the above discussion, the highest photoconductivity amplification (94.4) observed for AuNR−12.6 nm ZnO film can be attributed to the fully depleted nature of the ZnO, where electron injection from the AuNR results in the highest change in conductivity. The presence of electromagnetic hotspots can lead to a localized "bolometric" effect in the ZnO film, as has been observed for conduction in alkane molecules attached to Au nanoparticles.[24] The impact of AuNR density is weak within the parameter space tested. Although only modest enhancements from 1.34 to 1.40 are seen between low- and high-density AuNR−20.3 nm ZnO, similar enhancements are not observed between low (94.4) and high density (55.5) AuNR−12.6 nm ZnO films. It has been known that "hot" electron injection into insulating dielectrics present Coulombic barriers that affect sustained charge injection[25] and hence, high-density AuNR−ZnO nanocomposites may demonstrate limited photoresponse.

5. CONCLUSION

We demonstrate plasmon induced switching behavior from a metal to a semiconductor in AuNR−ZnO nanocomposite films. The metallic regime usually observed between 80 and 150 K switches to a semiconducting regime upon sub-bandgap white light illumination. The effect is the strongest (photoresponse = 94.4) for AuNR−12.6 nm ZnO film and decreases rapidly for AuNR 20.3 and 35.6 nm ZnO films. This effect is explained using a parallel circuit model of metallic and ZnO pathways where upon either thermal or light excitation, the ZnO

Table 1. Listing of Various Parameters for Pure ZnO and Low-Density Au −ZnO Nanocomposites under Dark and Light Illumination and for Various Thicknesses of ZnO Films

		pure ZnO		with AuNR			
ZnO thickness (nm)	illumination	max. photoresponse	E_a (meV)	max. photo response	$\rho_{metallic}$ (Ω)	α (K^{-1})	E_a (meV)
12.6 nm ZnO	dark		183		168×10^6	3×10^{-3}	137
	light	1.15	103	94.4			120
20.3 nm ZnO	dark		98		113×10^3	1.1×10^{-3}	81
	light	1.25	74	1.36			64
35.6 nm ZnO	dark		33		628	1.3×10^{-4}	72
	light	1.47	38	1.1			45

becomes the dominant conducting path. Although the thermal activation of ZnO conductivity is to be expected, direct evidence of plasmonically injected electrons from the AuNR to the ZnO is reported here. Activation energies are found to be ZnO thickness dependent varying from 120 meV for AuNR−12.6 nm ZnO to 45 meV for AuNR−35.6 nm ZnO.

■ ASSOCIATED CONTENT

Supporting Information

Experimental details on AuNR syntheses, AuNR attachment to glass substrates, white light spectral power intensity used in this experiment, AFM images of low-density AuNRs, low-density AuNRs with 12.6 nm ZnO, and the calculation for depletion width. This material is provided free of charge via the internet at http://pubs.acs.org/.

■ AUTHOR INFORMATION

Corresponding Author

*E-mail: parag.banerjee@wustl.edu.

Notes

The authors declare no competing financial interest.

■ ACKNOWLEDGMENTS

The authors thank the Washington University start-up funds, International Center for Advanced Renewable Energy and Sustainability (I-CARES) 2012 seed funding at Washington University, and SAFC Hitech for financial support. This work was performed in part at the Nano Research Facility (NRF), a member of the National Nanotechnology Infrastructure Network (NNIN), which is supported by the National Science Foundation under Grant ECS-0335765. Any opinions, findings, conclusions, or recommendations expressed in this material are those of the author(s) and do not necessarily reflect the views of the National Science Foundation. The authors acknowledge the support of shared user facilities of the Institute of Materials Science and Engineering (I-MSE).

■ REFERENCES

(1) Knight, M. W.; Sobhani, H.; Nordlander, P.; Halas, N. J. *Science* **2011**, *332*, 702−704.
(2) Atwater, H. A.; Polman, A. *Nat. Mater.* **2010**, *9*, 205−213.
(3) Lin, J.; Mueller, J. P. B.; Wang, Q.; Yuan, G.; Antoniou, N.; Yuan, X. C.; Capasso, F. *Science* **2013**, *340*, 331−334.
(4) Linic, S.; Christopher, P.; Ingram, D. B. *Nat. Mater.* **2011**, *10*, 911−921.
(5) Banerjee, P.; Conklin, D.; Nanayakkara, S.; Park, T. H.; Therien, M. J.; Bonnell, D. A. *ACS Nano* **2010**, *4*, 1019−1025.
(6) Funston, A. M.; Novo, C.; Davis, T. J.; Mulvaney, P. *Nano Lett.* **2009**, *9*, 1651−1658.
(7) Schuller, J. A.; Barnard, E. S.; Cai, W. S.; Jun, Y. C.; White, J. S.; Brongersma, M. L. *Nat. Mater.* **2010**, *9*, 193−204.
(8) Mubeen, S.; Lee, J.; Singh, N.; Kramer, S.; Stucky, G. D.; Moskovits, M. *Nat. Nanotechnol.* **2013**, *8*, 247−251.
(9) Mubeen, S.; Hernandez-Sosa, G.; Moses, D.; Lee, J.; Moskovits, M. *Nano Lett.* **2011**, *11*, 5548−5552.
(10) Lee, J.; Mubeen, S.; Ji, X.; Stucky, G. D.; Moskovits, M. *Nano Lett.* **2012**, *12*, 5014−5019.
(11) Kowalska, E.; Mahaney, O. O. P.; Abe, R.; Ohtani, B. *Phys. Chem. Chem. Phys.* **2010**, *12*, 2344−2355.
(12) Chang, S.; Li, Q.; Xiao, X. D.; Wong, K. Y.; Chen, T. *Energy Environ. Sci.* **2012**, *5*, 9444−9448.
(13) Tian, L. M.; Chen, E.; Gandra, N.; Abbas, A.; Singamaneni, S. *Langmuir* **2012**, *28*, 17435−17442.
(14) Abbas, A.; Tian, L. M.; Kattumenu, R.; Halim, A.; Singamaneni, S. *Chem. Commun.* **2012**, *48*, 1677−1679.
(15) Mayer, K. M.; Hafner, J. H. *Chem. Rev.* **2011**, *111* (6), 3828−3857.
(16) Vigderman, L.; Khanal, B. P.; Zubarev, E. R. *Adv. Mater.* **2012**, *24*, 4811−4841.
(17) Lee, K. S.; El-Sayed, M. A. *J. Phys. Chem. B* **2005**, *109*, 20331−20338.
(18) Orendorff, C. J.; Gearheart, L.; Jana, N. R.; Murphy, C. J. *Phys. Chem. Chem. Phys.* **2006**, *8*, 165−170.
(19) Oh, B. Y.; Kim, J. H.; Han, J. W.; Seo, D. S.; Jang, H. S.; Choi, H. J.; Baek, S. H.; Kim, J. H.; Heo, G. S.; Kim, T. W.; Kim, K. Y. *Curr. Appl. Phys.* **2012**, *12*, 273−279.
(20) Tseng, Z. L.; Kao, P. C.; Chen, Y. C.; Juang, Y. D.; Kuo, Y. M.; Chu, S. Y. *J. Electrochem. Soc.* **2011**, *158*, J310−J315.
(21) Melnick, D. A. *J. Chem. Phys.* **1957**, *26*, 1136−1146.
(22) Takahashi, Y.; Kanamori, M.; Kondoh, A.; Minoura, H.; Ohya, Y. *Jpn. J. Appl. Phys. 1* **1994**, *33*, 6611−6615.
(23) Takahashi, Y.; Masaaki, K.; Kondoh, A. *Jpn. J Appl. Phys. 1* **1994**, *33*, 5−7.
(24) Mangold, M. A.; Weiss, C.; Calame, M.; Holleitner, A. W. *Appl. Phys. Lett.* **2009**, *94*, 161104.
(25) Dimaria, D. J.; Cartier, E. *J. Appl. Phys.* **1995**, *78*, 3883−3894.